Front. Earth Sci. 2014, 8(4): 625–633
DOI 10.1007/s11707-014-0479-y

RESEARCH ARTICLE

Polarization signature from the FengYun-3 Microwave Humidity Sounder

Xiaolei ZOU (✉)[1], Xu CHEN[1,2], Fuzhong WENG[3]

1 Center of Data Assimilation for Research and Application, Nanjing University of Information Science & Technology, Nanjing 210044, China
2 Department of Earth, Ocean and Atmospheric Sciences, Florida State University, FL 32306, USA
3 National Environmental Satellite, Data & Information Service, National Oceanic and Atmospheric Administration, College Park, MD 20740, USA

Abstract Microwave Humidity Sounders (MHS) onboard NOAA-15, -16, -17, -18, -19, and EUMETSAT MetOp-A/B satellites provide radiance measurements at a single polarization state at any of five observed frequencies. The Microwave Humidity Sounder (MWHS) onboard the FengYun-3 (FY-3) satellite has a unique instrument design that provides dual polarization measurements at 150 GHz. In this study, the MWHS polarization signal was investigated using observed and modeled data. It is shown that the quasi-polarization brightness temperatures at 150 GHz display a scan angle dependent bias. Under calm ocean conditions, the polarization difference at 150 GHz becomes non-negligible when the scan angle varies from 10° to 45° and reaches a maximum when the scan angle is about 30°. Also, the polarization state is sensitive to surface parameters such as surface wind speed. Under clear-sky conditions, the differences between horizontal and vertical polarization states at 150 GHz increase with decreasing surface wind speed. Therefore, the polarization signals from the cross-track scanning microwave measurements at window channels contain useful information about surface parameters. In addition, the availability of dual polarization measurements allows a one-to-one conversion from antenna brightness temperature to sensor brightness temperature if a cross-polarization spill-over exists.

Keywords Microwave Humidity Sounder (MWHS), polarization, remote sensing, surface properties

1 Introduction

The FY-3 satellite series is a new generation of Chinese polar-orbiting satellites, with FY-3A and FY-3B successfully launched on May 27, 2008 and December 5, 2010, respectively. FY-3A is a morning satellite, with an equatorial crossing time (ECT) around 10:00 am. FY-3B is an afternoon satellite with ECT around 2:00 pm. All FY-3A/B satellites carry onboard 11 instruments, providing atmospheric sounding and other environmental observational data (Zhang et al., 2009). There are three microwave instruments including the Microwave Temperature Sounder (MWTS), the Microwave Humidity Sounder (MWHS), and the Microwave Radiation Imager (MWRI). The two microwave instruments onboard FY-3A/B, MWTS, and MWHS, are similar, but not identical, in channel specification to the AMSU-A and MHS onboard the NOAA's Polar-Orbiting Environmental Satellite (POES) series, which started in 1998 (Goodrum et al., 2009; Zou et al., 2012b). The MWTS onboard FY-3A/B has only four channels located at the atmospheric oxygen absorption band near 50–60 GHz and is mainly designed to provide information on atmospheric temperature profiles. MWTS channels 1–4 correspond to AMSU-A channels 3, 5, 7, and 9. The MWHS onboard has five channels, with three channels located at the 183 GHz water vapor absorption line, the same as the Microwave Humidity Sounder (MHS). The two MWHS window channels are located at 150 GHz with horizontal polarization and vertical polarization, which are different from the two MHS window channels located at 89 and 157 GHz with single polarization. MWRI has most of the frequencies of the Advanced Microwave Scanning Radiometer–EOS (AMSR-E) onboard the NASA Aqua satellite except for the C-band (6.9 GHz).

The FY-3 series will significantly contribute to the Global Environmental Observing System of Systems (GEOSS). The Earth's atmosphere can be observed more frequently than without Chinese satellites. A preliminary evaluation of instrument performance through a compar-

Received December 18, 2013; accepted July 1, 2014

E-mail: xzou@fsu.edu

ison with data from NOAA, MetOp, and the NASA Aqua satellite data revealed that data from MWTS, MWHS, and MWRI were of good quality (Guan et al., 2011; Yang et al., 2011; Wang et al., 2012; Wang and Zou 2012; Zou et al., 2012a; Zou et al., 2012b; Zou et al., 2012c). In this study, we investigated the polarization differences of measurements between two MWHS window channels and investigated the potential value for satellite data assimilation and calibration.

It is well known that microwave radiation emitted from oceans in the low frequency range, from 6 GHz to 37 GHz, exhibits an obvious difference between vertical and horizontal polarization states (Wilheit, 1979; Sasaki et al., 1987; Ruf, 1998; Rosenkranz, 1992). Generally speaking, for microwave radiation over calm ocean surfaces under clear-sky conditions, brightness temperature at vertical polarization increases and that at horizontal polarization decreases with incident angle from nadir until it reaches Brewster's angle (also known as the polarization angle). In 1978, the scanning multichannel microwave radiometer (SMMR) was flown on the Seasat and Nimbus-7 satellites and lasted from 25 October 1978 until 20 August 1987. The SMMR provided measurements of dual-polarized microwave radiances at 6.63, 10.69, 18.0, 21.0, and 37.0 GHz with the antenna beam intersecting the Earth's surface at an incidence angle of 50.1° (Gloersen et al., 1984). Since then, the Special Sensor Microwave Imager (SSM/I) was flown onboard the US Air Force Defense Meteorological Satellite Program (DMSP) satellites with frequencies and local incident angle similar to those of SMMR (Derksen et al., 2003; Dai and Che, 2009). Many microwave imagers have been launched recently, following SMMR and SSM/I. Other microwave imager sensors onboard polar-orbiting meteorological satellites include the AMSR-E, the WindSat radiometer onboard the Department of Defense (DoD) Coriolis satellite, the MWRI onboard FY-3 series satellites, and the successor of AMSR-E, AMSR-2, onboard the Global Change Observation Mission 1st-Water (GCOM-W1) satellite. All SSM/I, SSMIS, WindSat, AMSR-E, MWRI, and AMSR-2 instruments are conical scanning radiometers, which are characterized by a constant scan angle for all field-of-views (FOVs). Measurements from dual polarization had thus been used for remote sensing of wind speeds near the ocean surface (Hollinger, 1990; Wentz, 1991; Wentz, 1997; Shibata, 2006; Mitnik and Mitnik, 2010).

Different from conically scanning total power passive microwave radiometers SMMR, SSM/I, AMSR-E, MWRI, and AMSR-2, MWHS is a cross-track scanning sounder. The antenna scans from $-53.38°$ to 53.38°, providing a total of 98 FOVs within this scan range. MWHS has a nominal instantaneous FOV of 15 km at nadir. The swath width of MWHS is about 2700 km. For a cross-track scanning instrument, the polarization state varies with scan angle (Thompson et al., 1998). It is purely vertical or horizontal only at the nadir. The polarization signals contained in the new radiance observations at 150 GHz with two polarization states at different scan angles are not understood well and were the subject of this study.

2 Characterization of the MWHS

The MWHS onboard FY-3B is a cross-track total power microwave radiometer. It has five channels in the frequency range of 150 GHz to 191 GHz. Three humidity sounding channels are located near the water vapor absorption line at 183.3 GHz, with each channel having two pass-bands of a frequency offset from the center of ±1, ±3, and ±7 GHz, respectively. These channels have a pure vertical polarization at nadir. Two window channels are located at 150 GHz with quasi-vertical (V) and quasi-horizontal (H) polarization.

In a normal operational mode for MWHS on orbit, two flat reflectors, perpendicular to the flight track, rotate and scan the earth, reflecting radiation to two offset-fed parabolic antennas. The stable parabolic antennas collect the radiation and send it to a corrugated feed horn (Gu et al., 2012). Then, polarization is segregated and frequency is divided by a quasi-optical system to obtain the observational data expressed in the form of counts. The earth scanning aperture angle of MWHS is $\pm53.35°$ and the sampling distance is 1.1°, resulting in a total of 98 FOVs. The scan period is 8/3 s. A total of seven platinum resistance thermometers (PRTs) are placed in the internal blackbody for monitoring the blackbody temperature, of which five are active and two are for backup. The space calibration scan angle is 107.1°. The antennas scan the space and internal blackbody in a uniform speed to obtain three sets of space view data and three sets of internal blackbody view data, respectively. These space view and internal blackbody data are used to complete the on-orbit two-point calibration for obtaining MWHS antenna temperatures.

FY-3A/B MWHS receivers are designed as the double sideband type. The stability of frequency is 50 MHz. The main beam efficiency of the antenna is greater than 95.0%, and cross-polarization beam efficiency is lower than -20dB. The differences of channel frequency and polarization state between MWHS and MHS are provided in Table 1. In a scanning period, the MWHS antenna scans the earth, space, and internal blackbody target in a uniform speed, but moves with acceleration and deceleration in two fast switch sections.

3 Theoretical description

As the MWHS antenna scans across from a limb position to nadir, and then to a limb position on the other side, it

Table 1 Frequency and polarization differences between MWHS and MHS channels

Channel	1	2	3	4	5
MWHS	150 h	150 v	183.31±1 v	183.31±3 v	183.31±7 v
MHS	89.0 v	157.0 v	183.31±1 h	183.31±3 h	190.31 v

receives signals from both horizontal and vertical polarizations and obtains the so-called quasi-vertical (T_a^{Qv}) and quasi-horizontal (T_a^{Qh}) antenna temperature (Choudhury et al., 1992; Bauer and Schluessel, 1993; Lei et al., 2008). The MWHS measured quasi-vertical and quasi-horizontal antenna temperatures (T_a^{Qv}, T_a^{Qh}) are related to the quasi-vertical and quasi-horizontal sensor brightness temperatures (T_b^{Qv}, T_b^{Qh}) according to the following equations (Weng et al., 2013),

$$T_a^{Qv} = \eta_{me}^{vv} T_b^{Qv} + \eta_{me}^{hv} T_b^{Qh} + S_a^{Qv}, \tag{1a}$$

$$T_a^{Qh} = \eta_{me}^{hh} T_b^{Qh} + \eta_{me}^{vh} T_b^{Qv} + S_a^{Qh}, \tag{1b}$$

where η_{me}^{vv} and η_{me}^{hh} are the co-polarized antenna beam efficiencies; η_{me}^{hv} and η_{me}^{vh} are the cross-polarized antenna beam efficiencies; and S_a^{Qv} and S_a^{Qh} are the near field radiation term antenna temperatures of the satellite platform seen by the side-lobes. For a normal scan of MWHS, the first two terms in Eq. (1) are the earth radiation entering into the receiver system through the main beam, which is determined by 2.5 times the half-power beam width, and the last term is the radiation scattered and emitted from the satellite platform and/or antenna reflector to the receiver.

Based on Eq. (1) it is seen that the sensor brightness temperature (T_b^{Qv}, T_b^{Qh}) can be uniquely determined from simultaneously measuring the antenna brightness temperatures at both polarizations at the same frequency (T_a^{Qv}, T_a^{Qh}) if (S_a^{Qv}, S_a^{Qh}) are negligible or known. With single polarization measurements such as MHS channels, the conversion from antenna temperatures to sensor brightness temperatures becomes non-unique if the antenna subsystem has a significant spill-over from cross-polarization (i.e., $\eta_{me}^{hv} \neq 0$, $\eta_{me}^{vh} \neq 0$).

The quasi-horizontal and quasi-vertical sensor brightness temperatures from a cross-tracking radiometer, T_b^{Qv} and T_b^{Qh}, are related to the pure polarized brightness temperatures T_b^v and T_b^h as follows:

$$T_b^{Qv} = T_b^v \cos^2\theta + T_b^h \sin^2\theta, \tag{2a}$$

$$T_b^{Qh} = T_b^v \sin^2\theta + T_b^h \cos^2\theta, \tag{2b}$$

where θ is the scan angle. In the Community Radiative Transfer Model (CRTM) developed at the Joint Center for Satellite Data Assimilation (JCSDA) (Han et al., 2006), pure polarized brightness temperatures T_b^v and T_b^h are first calculated, which are then converted to quasi-vertical and quasi-horizontal sensor temperatures T_b^{Qv} and T_b^{Qh} using Eq. (2).

Figure 1 shows the variations of CRTM-simulated sensor brightness temperatures T_b^{Qv} and T_b^{Qh} at 150.00 GHz with scan angle. The surface emissivity model used in the simulation is an improved fast microwave water emissivity model developed by JCSDA (Liu Q et al., 2011). It is seen that the sensor brightness temperature at horizontal polarization (T_b^{Qh}) varies differently from that at vertical polarization (T_b^{Qv}) at a frequency of 150 GHz as shown in Fig. 1. The sensor brightness temperature at horizontal polarization slightly decreases with scan angle from 0 to about 22° and then increases rapidly with scan angle, while brightness temperature at vertical polarization increases quite rapidly with scan angle till about a 38° scan angle and then increases only slightly with scan angle. Variations of the differences of the sensor brightness temperature difference between horizontal and vertical polarization channels are provided in Fig. 2. The largest positive difference between horizontal and vertical polarizations appears near the 53° scan angle. There also exists a maximum negative difference between horizontal and vertical polarization channels at the 30° scan angle, where

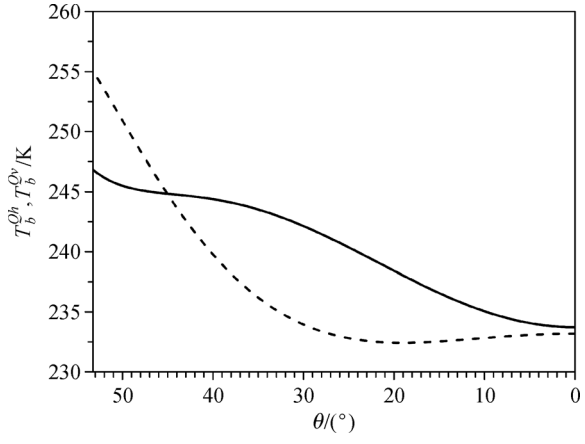

Fig. 1 Variations of sensor brightness temperatures of quasi-horizontal polarization (T_b^{Qh}, dashed line) and quasi-vertical polarization (T_b^{Qv}, solid line) channels at a frequency of 150.0 GHz (e) with scan angle using a middle latitude winter profile over ocean

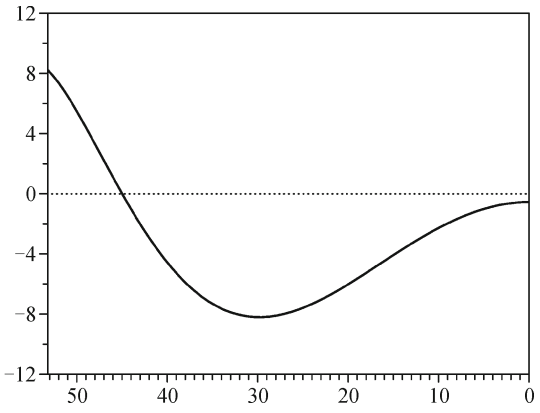

Fig. 2 Sensor brightness temperature difference between quasi-horizontal and vertical polarization channels ($\Delta T_b = T_b^{Qh} - T_b^{Qv}$) with frequency of 150 GHz at different scan angles shown in Fig. 1

brightness temperature at horizontal polarization is about 8 K smaller than brightness temperature at vertical polarization.

4 Real-data analysis

FY-3B MWHS observations and the National Centers for Environmental Prediction (NCEP) global forecast system (GFS) 6-h forecast surface wind fields during a one and half month period from 0000 UTC March 1 to 1800 UTC April 14, 2011 were used in this study.

Figure 3 provides scatter plots of MWHS channels 1 and 2 sensor brightness temperature observations at the 1st, 23rd, 49th, and 98th FOV only for data points with surface wind speed less than 3 $m \cdot s^{-1}$. There are two reasons for choosing data over areas with wind speeds less than 3 $m \cdot s^{-1}$. The main reason is for clear-sky radiance assimilation using MWHS data. If the sensitivity of polarization to surface wind speed is not negligible, adjustments in surface wind variables are expected from MWHS radiance assimilation. The second reason is to avoid the polarization effect of clouds, since polarization signals can be generated by the strong scattering effects of non-spherical ice cloud particles in measurements from quasi-vertical and quasi-horizontal polarization at the 150 GHz frequency of MWHS window channels 1 and 2. This study was limited to the investigation of the sensitivity of polarization differences to wind speed at different scan angles. The results indicate that a branch exists where brightness temperatures at the horizontal polarization (channel 1) are larger than at channel 2 at the 1st and 98th FOVs. At the 23rd FOV, there is a branch where brightness temperatures at the horizontal polarization (channel 1) are smaller than those at channel 2. For the 49th FOV, channel 1 correlates very well with channel 2. The scan dependence of brightness temperature differences between channels 1 and 2 within 45°N–50°N and mean differences for both observations and model simulations are shown in Fig. 4. As expected, the modeled polarization differences (Fig. 4 (a)) are negligible at nadir over calm oceans, when wind speed is less than 3 $m \cdot s^{-1}$. The difference between channels 1 and 2 switches its sign from the 8th to the 9th FOV and from the 90th to 91th FOV, resulting in a "W-shaped" mean difference distribution between channels 1 and 2 from both observations and model simulations. The mean differences between channels 1 and 2 from MWHS observations (Fig. 4(b)) are similar to those of model simulations (Fig. 4(a)) except for a large spread, a nonzero mean at nadir, and smaller mean values at the largest scan angles.

The mean and standard deviation of the brightness temperature differences between MWHS channels 1 and 2 for MWHS observations and model simulations during the period from 0000 UTC March 1 to 1800 UTC April 14, 2011 are shown in Fig. 5. The polarization differences between MWHS channel 1 (e.g., horizontal polarization) and MWHS channel 2 (i.e., vertical polarization) are largest and positive (10 K) at the largest scan angle. The second largest differences are negative and located near the ±37° scan angles. Polarization differences are smallest near nadir. These results are consistent with theoretical simulations of the differences between horizontal and vertical polarizations at 150 GHz (Figs. 1 and 2). The polarization differences from MWHS observations are asymmetrical (Figs. 5(a) and (c)) and those from model simulations are symmetrical (Fig. 5(b) and (d)), reflecting probably the contribution of the radiation scattered and emitted from the satellite platform to the receiver (i.e., S_a^{Qv} and S_a^{Qh} in Eq. (1)). The standard deviations are larger over regions where the mean differences are large.

Finally, polarization sensitivities to surface wind speed under clear-sky conditions were examined. Clear-sky MWHS FOVs were found by requiring that 1) they collocate with AMSU-A and MHS measurements from NOAA-18 with a temporal difference being less than 1 h and a spatial distance being less than 30 km; and 2) the collocated AMSU-A derived cloud liquid water path (LWP) or the collocated ice water path (IWP) is less than 0.01 $kg \cdot m^{-2}$. More than 700 collocated samples were found at each FOV in March 2011. Figure 6 presents scatter plots of brightness temperature differences between the horizontal (MWHS channel 1) and vertical polarizations (MWHS channel 2) at FOV 20 for data on FY-3B ascending orbits in March 2011 in three arbitrarily chosen domains. The corresponding mean and standard deviation values calculated at a wind speed interval of 3 $m \cdot s^{-1}$ are also shown in Fig. 6. It is seen that the polarization differences decrease with increasing surface wind speed. The brightness temperatures at the horizontal polarization state can be more than eight degrees lower than the brightness temperatures at the vertical polarization state.

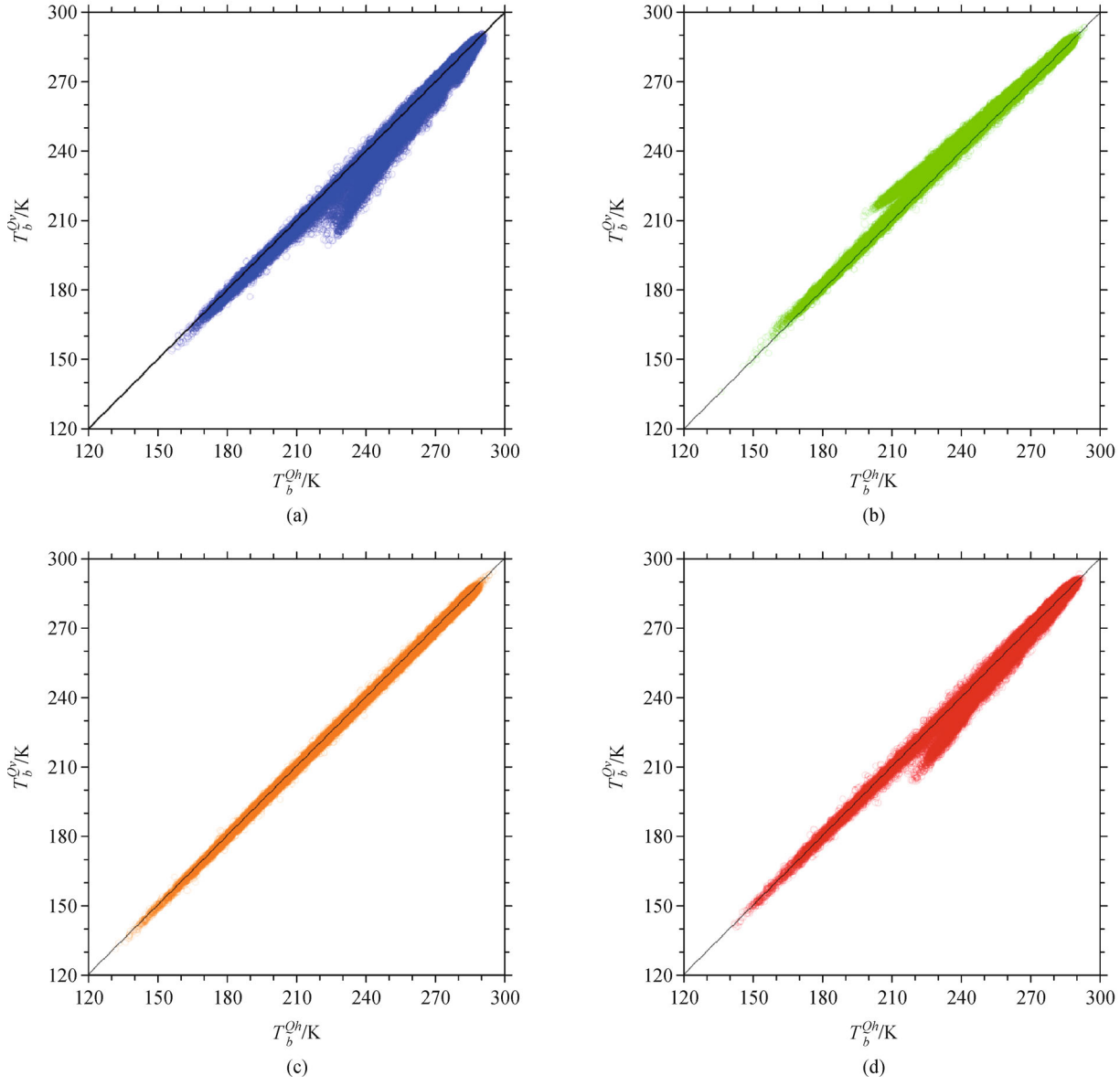

Fig. 3 Scatter plots of MWHS channels 1 and 2 sensor brightness temperatures at the 1st (a), 23rd (b), 49th (c), and 98th (d) FOVs, of which the scan angles are 53.35°, 29.15°, 0.55°, and 53.35°, respectively, during 0000 UTC March 1 to 1800 UTC April 14, 2011 only for data with surface wind speed less than 3 $m \cdot s^{-1}$

The scan dependence of the variations of the mean differences of brightness temperature between the horizontal (channel 1) and vertical (channel 2) states with surface wind speed are provided in Fig. 7. The polarization differences are smallest at FOVs 10 and 11, which are the two FOVs with their scan angles closest to 45°. As the scan angle varies further from 45°, the sensitivity of the polarization signature increases. When surface wind speed is smallest, the polarization differences are largest. It is therefore concluded that the polarization differences of microwave humidity measurements at 150 GHz from FY-3B MWHS channels 1 and 2 contain useful information about surface wind speed.

5 Summary and conclusions

Traditionally only a single polarization is measured for AMSU-A and MHS. The MWHS onboard FY-3A/B provides, for the first time, measurements of dual polarization at 150 GHz. It allows an investigation of the benefit for cross-track radiometers such as MHS and

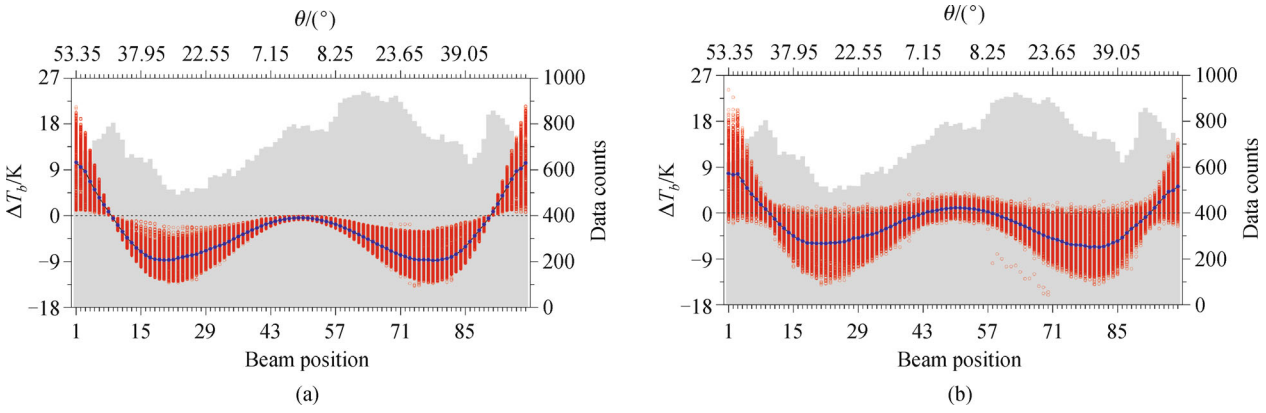

Fig. 4 Sensor brightness temperature differences between MWHS channels 1 and 2 ($\Delta T_a = T_a^{Qh} - T_a^{Qv}$, red circles), mean difference (blue curve), and data counts (gray bar) from (a) model simulations and (b) observations within 45°N–50°N with collocated surface wind speed less than 3 $m \cdot s^{-1}$. All data from 0000 UTC March 1 to 1800 UTC April 14, 2011 are used

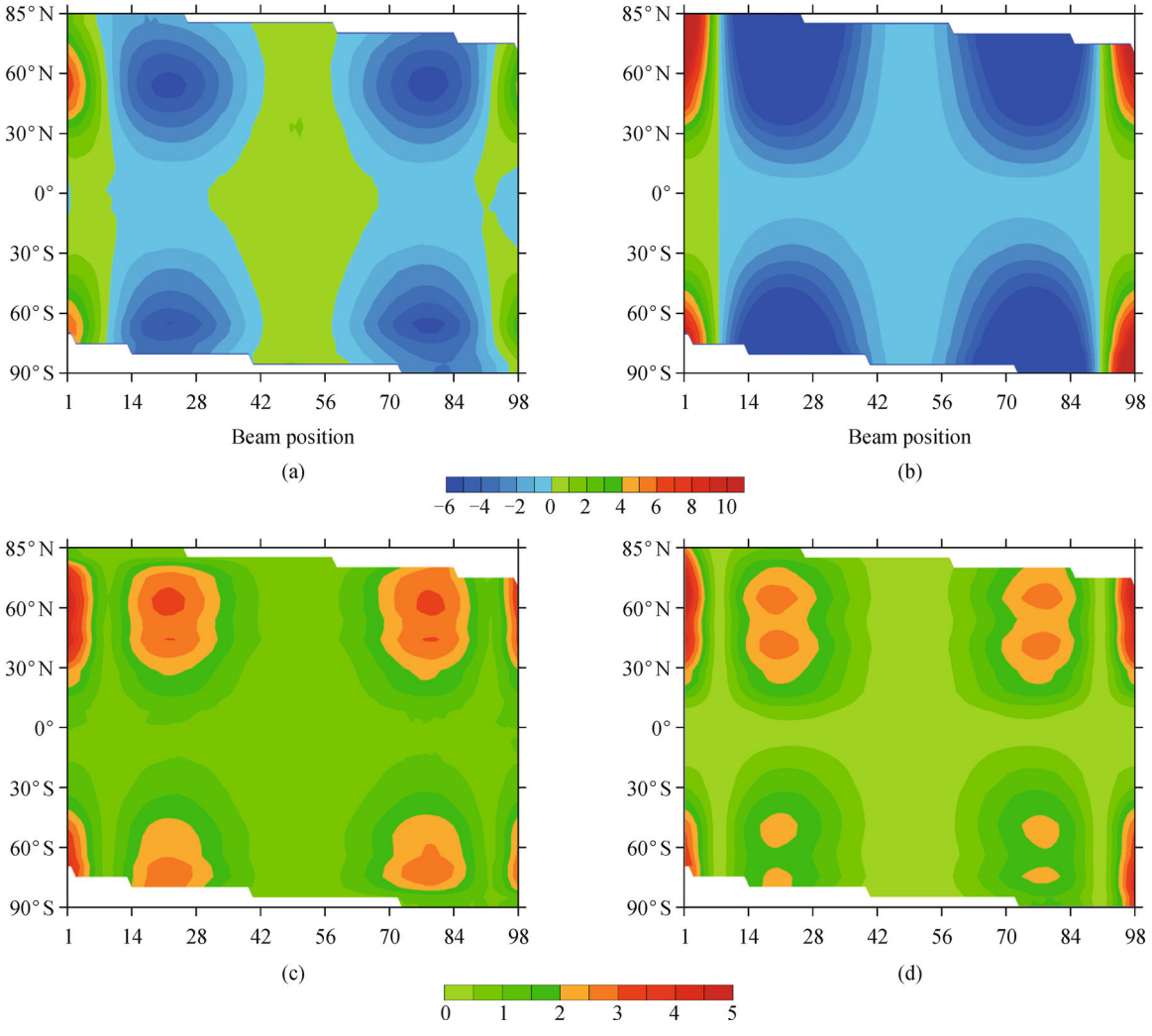

Fig. 5 Latitudinal dependence of (a)-(b) mean and (c)-(d) standard deviation of the sensor brightness temperature differences between MWHS channels 1 and 2 for MWHS observations (left panels) and simulated sensor brightness temperature difference (right panels) from 0000 UTC March 1 to 1800 UTC April 14, 2011

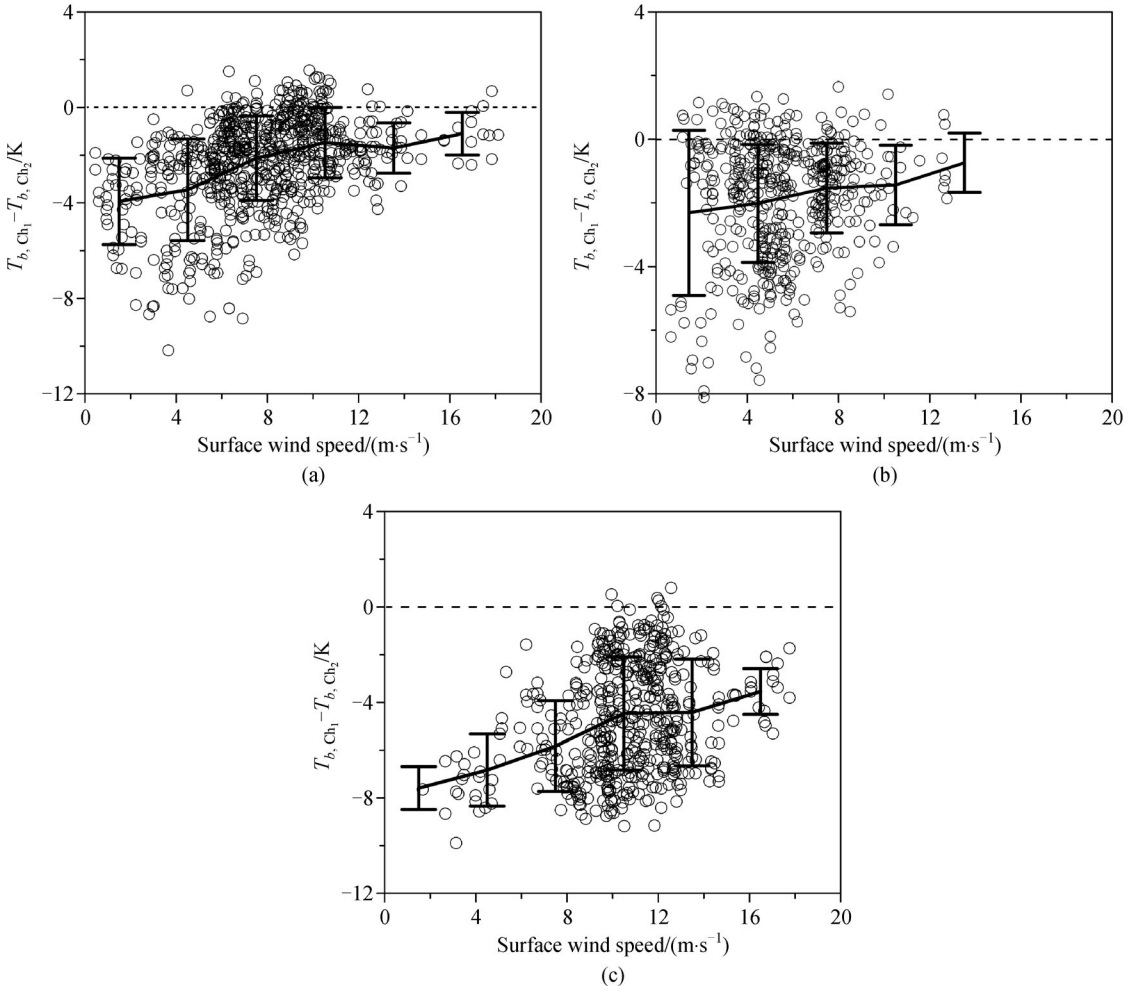

Fig. 6 Scatter plots of brightness temperature differences between MWHS/FY-3B channels 1 and 2 at FOV 20 for observations on ascending orbits in March 2011 in clear-sky conditions within three arbitrarily chosen domains: (a) 30°N–40°N, 170°W–130°W, (b) 40°S–30°S, 140°W–100°W, and (c) 60°S–50°S, 180°W–140°W. The mean (thick solid) and standard deviation (vertical thin line) calculated at a wind speed interval of 3 m·s^{-1} are also shown

AMSU-A of measuring both horizontal and vertical polarizations at the same frequency. Using model simulations, it was shown that scan-angle dependences of brightness temperatures at 150 GHz horizontal and vertical polarizations are similar to those at lower frequency AMSU-A channels, but of a slightly smaller magnitude. The largest polarization differences are found at scan angles of 53.35° and 33°, respectively, but with opposite signs. The polarization differences at 150 GHz based on MWHS observations are shown to be sensitive to surface wind speed. It was also pointed out that the availability of dual polarization observations at microwave temperature- and humidity-sounding frequencies would also make the conversion from antenna temperature to sensor brightness temperature a well-determined inverse problem. Further investigation will be carried out to assess the calibration accuracy with a dual polarization versus a single polarization.

This study was limited to examining the sensitivity of polarization to surface wind speed. Measurements from quasi-vertical and quasi-horizontal polarization can be impacted by not only surface wind speed, but also other parameters such as salinity and wind direction. At the 150 GHz frequency of MWHS window channels 1 and 2, measurements from quasi-vertical and quasi-horizontal polarization can also be strongly scattered by non-spherical ice cloud particles, generating polarization signals. Future work is planned for investigating the sensitivity of polarization differences to wind direction, salinity, and cloud types using FY-3B MWHS data.

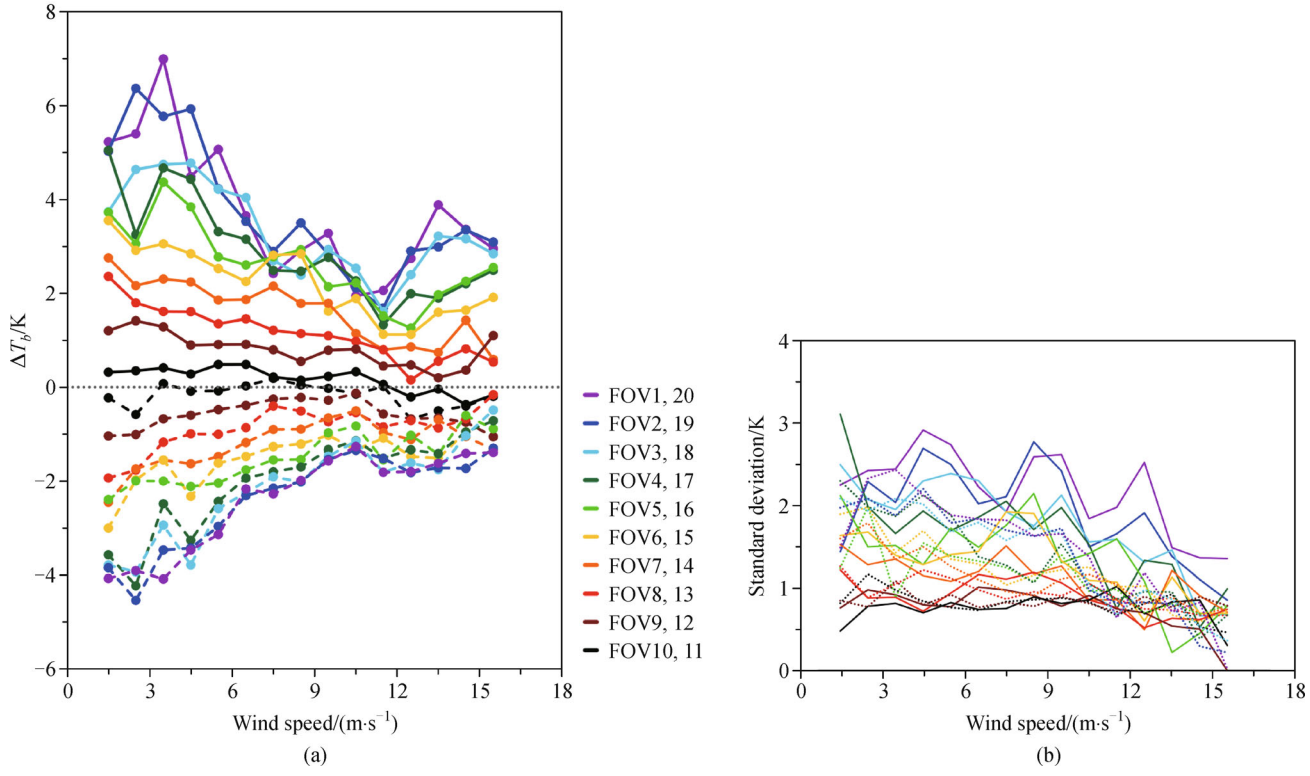

Fig. 7 Variation of the (a) mean and (b) standard deviation of the sensor brightness temperature difference between horizontal and vertical polarization states at 150 GHz frequency with surface wind speed, using data within 30°N–40°N and 130°W–170°W under clear-sky conditions in March 2011. The first to tenth FOVs are indicated by filled circles in (a) and solid lines in (b) and FOVs 11–20 by open circles in (a) and dotted lines in (b)

Acknowledgements This work was jointly supported by Chinese Ministry of Science and Technology Project 2010CB951600, and Chinese Ministry of Finance Project GYHY200906006.

References

Bauer P, Schluessel P (1993). Rainfall, total water, ice water, and water vapor over sea from polarized microwave simulations and special sensor Microwave/Imager data. J Geophys Res, D, Atmospheres, 98 (D11): 20737–20759

Choudhury B J, Major E R, Smith E A, Becker F (1992). Atmospheric effects on SMMR and SSM/1 37 GHz polarization difference over the sahel. Int J Remote Sens, 13(18): 3443–3463

Dai L, Che T (2009). Cross-platform calibration of SMMR, SSM/I and AMSR-E passive microwave brightness temperature. In: Proceedings of SPIE 7841, Sixth International Symposium on Digital Earth: Data Processing and Applications, 7841(03) DOI: 10.1117/12.873150

Derksen C, Walker A, LeDrew E, Goodison B (2003). Combining SMMR and SSM/I data for time series analysis of central north American snow water equivalent. J Hydrometeorol, 4(2): 304–316

Gloersen P, Cavalieri D J, Chang A T C, Wilheit T T, Campbell W J, Johannessen O M, Katsaros K B, Kunzi K F, Ross D B, Staelin D, Windsor E P L, Barath F T, Gudmandsen P, Langham E, Ramseier R O (1984). A summary of results from the first NIMBUS 7 SMMR observations. J Geophys Res, D, Atmospheres, 89(D4): 5335–5344

Goodrum G, Kidwell K B, Winston W (2009). NOAA KLM User's Guide. National Oceanic and Atmospheric Administration

Gu S, Guo Yang, Wang Z, Lu N (2012). Calibration analyses for sounding channels of MWHS onboard FY-3A. IEEE Trans Geosci Rem Sens, 50(12): 4885–4891

Guan L, Zou X, Weng F, Li G (2011). Assessments of FY-3A Microwave Humidity Sounder (MWHS) measurements using NOAA-18 Microwave Humidity Sounder (MHS). J Geophys Res, 116(D10): D10106

Han Y, Delst P V, Liu Q, Weng F, Yan B, Treadon, Derber J (2006). JCSDA Community Radiative Transfer Model (CRTM)-Version 1. NOAA Tech. Rep. NESDIS 122: 40

Hollinger J P, Peirce J L, Poe G A (1990). SSM/I instrument evaluation. IEEE Trans Geosci Rem Sens, 28(5): 781–790

Lei L, Zou J, Mao Z (2008). Improving ocean surface wind speed retrieval from SSM/I data by channel combinations. In: Proceeding of SPIE Remote Sensing of Clouds and the Atmosphere 7017(16) DOI: 10.1117/12.799763

Liu Q, Weng F, English S J (2011). An improved fast microwave water emissivity model. IEEE Trans Geosci Rem Sens, 49(4): 1238–1250

Mitnik L M, Mitnik M L (2010). AMSR-E advanced wind speed retrieval algorithm and its application to marine weather systems. Geoscience and Remote Sensing Symposium (IGARSS), 2010 IEEE International, 3224–3227

Rosenkranz P W (1992). Rough-sea microwave emissivities measured with the SSM/I. IEEE Trans Geosci Rem Sens, 30(5): 1081–1085

Ruf C S (1998). Constraints on the polarization purity of a stokes microwave radiometer. Radio Sci, 33(6): 1617–1639

Sasaki Y, Asanuma I, Muneyama K, Naito G, Suzuki T (1987). The dependence of sea-surface microwave emission on wind speed, frequency, incidence angle, and polarzation over the frequency range from 1 to 40 GHz. IEEE Trans Geosci Rem Sens, 25(2): 138–146

Shibata A (2006). A wind speed retrieval algorithm by combining 6 and 10 GHz data from Advanced Microwave Scanning Radiometer: Wind speed inside hurricanes. J Oceanogr, 62(3): 351–359

Thompson D R, Elfouhaily T M, Chapron B (1998). Polarization ratio for microwave backscattering from the ocean surface at low to moderate incidence angles. In: Proceeding of Geoscience and Remote Sensing Symposium, 1998 IEEE International, 3: 1671–1673 DOI: 10.1109/IGARSS.1998.692411

Wang X, Zou X (2012). Quality assessments of Chinese FengYun-3B Microwave Temperature Sounder (MWTS) measurements. IEEE Transcation on Gescience and Remote Sensing, 50(12): 4875–4884

Wang X, Zou X, Weng F, You R (2012). An assessment of the FY-3A microwave temperature sounder using the NCEP numerical weather prediction model. IEEE Transcation on Gescience and Remote Sensing, 50(12): 4860–4874

Weng F, Yang H, Zou X (2013). On convertibility from antenna to sensor brightness temperature for ATMS. IEEE transaction on Geoscience and Remote Sensing, 10(4): 771–775

Wentz F J (1991). A simplified wind vector algorithm for satellite scatteromete. J Atmos Ocean Technol, 8(5): 697–704

Wentz F J (1997). A well-calibrated ocean algorithm for special sensor microwave / imager. J Geophys Res, 102(C4): 8703–8718

Wilheit T T (1979). A model for the microwave emissivity of the ocean's surface as a function of wind speed. IEEE Trans Geosci Electron, 17 (4): 244–249

Yang H, Weng F, Lv L, Lu N, Liu G, Bai M, Qian Q, He J, Xu H (2011). The FengYun-3 Microwave Radiation Imager on-orbit verification. IEEE Trans Geosci Rem Sens, 49(11): 4552–4560

Zhang P, Yang J, Dong C, Lu N, Yang Z, Shi J (2009). General introduction on payloads, ground segment and data application of Fengyun 3A. Front Earth Sci China, 3(3): 367–373

Zou X, Ma Y, Qin Z (2012a). FengYun-3B Microwave Humidity Sounder (MWHS) data noise characterization and filtering using principle component analysis. IEEE Trans Geosci Rem Sens, 50(12): 4892–4902

Zou X, Wang X, Weng F, Li G (2012b). Assessments of Chinese FengYun Microwave Temperature Sounder (MWTS) measurements for weather and climate applications. J Atmos Ocean Technol, 28 (10): 1206–1227

Zou X, Zhao J, Weng F, Qin Z (2012c). Detection of radio-frequency interference signal over land from FY-3B Microwave Radiation Imager (MWRI). IEEE Trans Geosci Rem Sens, 50(12): 4994–5003